Supplementary Information

High electrical conductivity in $Ba_2In_2O_5$ brownmillerite based materials induced by design of Frenkel defect structure

Shigeharu Ito,[a, b] Toshiyuki Mori,*[a] Pengfei Yan,[a] Graeme Auchterlonie,[c]

John Drennan,[c] Fei Ye,[d] Keisuke Fugane[a, e] and Takaya Sato[b]

[a] Solid Oxide Fuel Cell Materials Design Group, **G**lobal **R**esearch Center for **E**nvironment and **E**nergy based on **N**anomaterials Science (GREEN), **N**ational **I**nstitute for **M**aterials **S**cience (NIMS), 1-1 Namiki, Tsukuba, Ibaraki 305-0044 Japan

[b] Department of Creative Engineering, Chemical and Biological course, National Institute of Technology, Tsuruoka College, 104 Sawada, Inoka, Tsuruoka, Yamagata, 997-8511 Japan

[c] Centre for Microscopy and Microanalysis, The University of Queensland, St. Lucia, Brisbane, Qld 4072, Australia

[d] School of Material Science and Engineering, Dalian University of Technology, 2 Linggong Road, Dalian 116024, China

e DENSO Corporation, 1-1 Showa-cho, Kariya, Aichi 448-8661, Japan

Corresponding author:

*Email: MORI.Toshiyuki@nims.go.jp, Tel: +81-29-860-4395, Fax: +81-29-860-4712

Figure S1 shows the data of Rietveld analysis of XRD for $Ba_2In_2O_5$ at room temperature. The characteristic super-lattice peaks of orthorhombic $Ba_2In_2O_5$ were clearly observed in Figure S1(ⅰ).
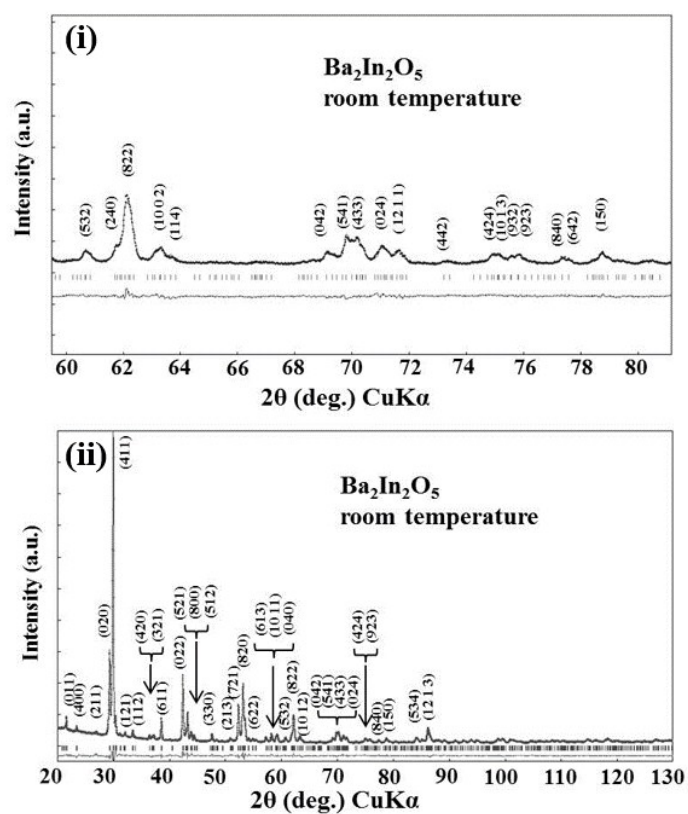

Figure S1. Rietveld analysis of XRD for $Ba_2In_2O_5$ at room temperature. (ⅰ): 2θ range ($60^o \leqq 2\theta \leqq 80^o$), (ⅱ): 2θ range ($20^o \leqq 2\theta \leqq 130^o$).

Table S1 summarized the refined structural parameters of $Ba_2In_2O_5$ at room temperature shown in Figure S1..

Table S1. Refined structural parameters of $Ba_2In_2O_5$ at room temperature.

$Ba_2In_2O_5$

Atom	Site	Occupancy	x	y	z
Ba	8c	1.00	0.61	0.51	0.00
In1	4a	1.00	0.00	0.00	0.05
In2	4b	1.00	0.25	0.56	0.48
O1	8c	1.00	0.98	0.25	0.25
O2	8c	1.00	0.13	0.07	0.04
O3	4b	1.00	0.25	0.67	0.15

Number of formula units per the unit cell	Lattice constants(Å)	Lattice volume(Å^3)
Z=4	a=16.713 b=6.089 c=5.954	V= 605.9

Space group *Ima2* (No.46), R_B=2.81(%), R_F=2.20(%), R_{WP}=5.27(%), S=1.87

Figure S2. presents XRD patterns taken from BIZZO-0.3 at room temperature and 1273K. As shown in Figure S2, the XRD peaks taken from BIZZO-0.3 at 1273K conspicuously shifted into low diffraction angle region (i.e. high d-value region) as compared with XRD peak observed for BIZZO-0.3 at room temperature. This is attributable to thermal expansion of the lattice of BIZZO-0.3 at 1273K.
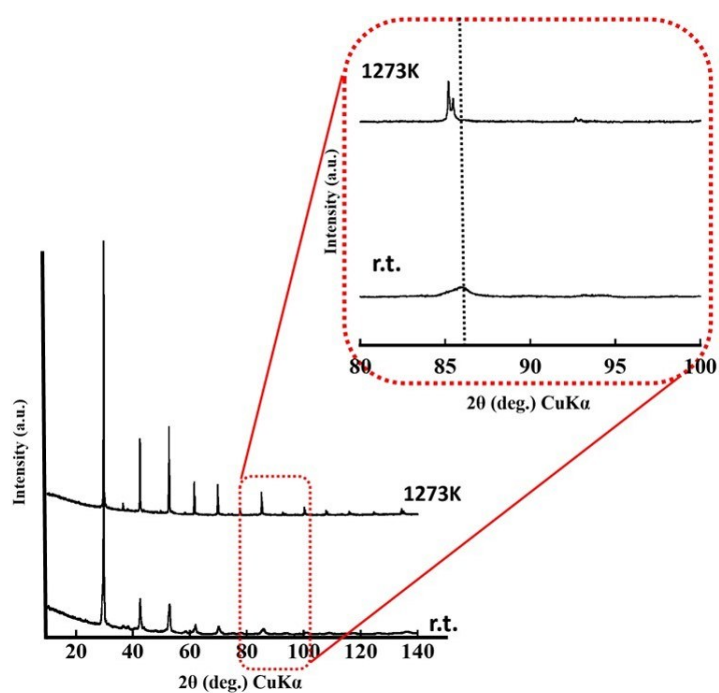

Figure S2. XRD pattern and its magnified pattern observed for BIZZO-0.3 at room temperature and 1273K.

On the basis of this result, we calculated the volume change of BIZZO-0.3 which is attributable to the thermal expansion of BIZZO-0.3 by using Rietveld analysis data as follows (see Table S2.);

Table S2. Lattice volumes estimated by Rietveld analysis data.

|	room temperature	1273K
Lattice volume ($Å^3$)	612.8 (see Table 3)	618.3 (see Table 4)

Volume change of BIZZO-0.3 lattice which is attributable to thermal expansion
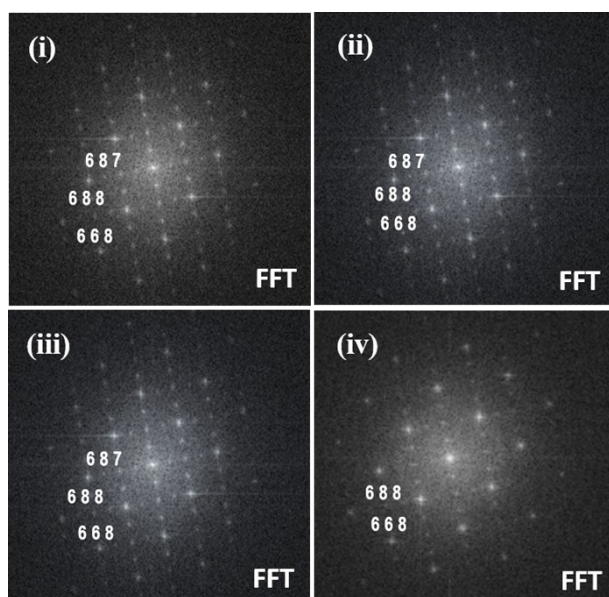
=   [(618.3 – 612.8) / 612.8] x 100

=   0.89 (vol%)

Figure S3. presents TEM images taken from $Ba_2In_{1.7}(Zn_{0.5},Zr_{0.5})_{0.3}O_5$. (a): <100> on zone image taken from $Ba_2In_{1.7}(Zn_{0.5},Zr_{0.5})_{0.3}O_5$, (b) FFT patterns of <100> on zone images and (c): IFFT images taken from FFT patterns.

(a)
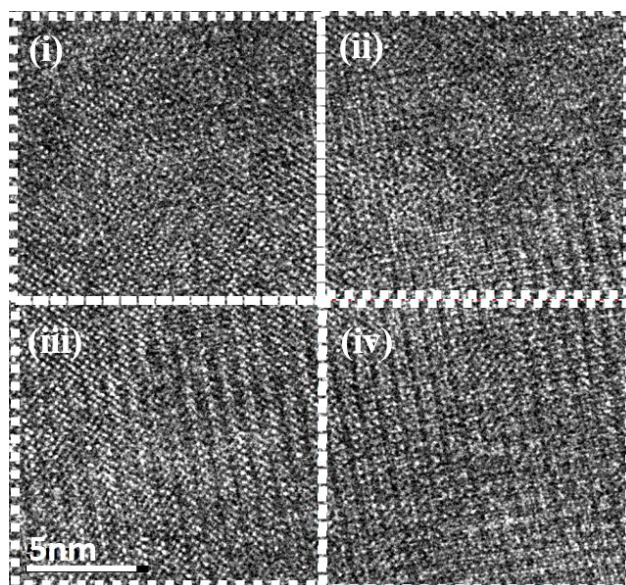
(b)

(c)

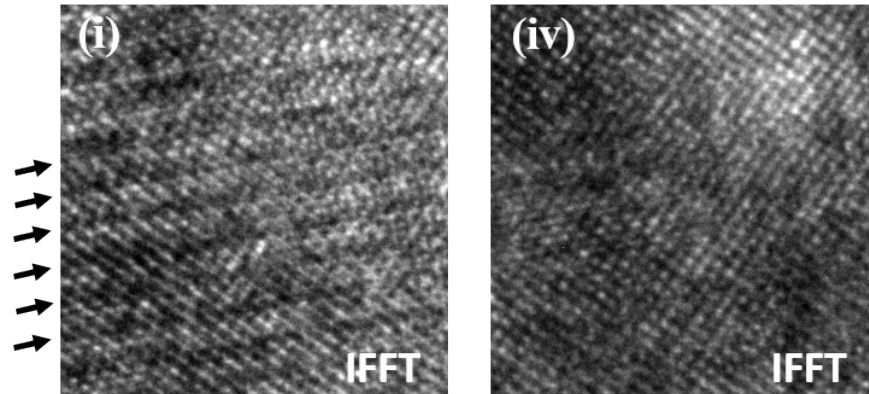Figure S3. (a)TEM <100> zone images ((i) − (iv)), (b)FFT <100> patterns and (c)IFFT <100> lattice fringe contrast taken from $Ba_2In_{1.7}(Zn_{0.5},Zr_{0.5})_{0.3}O_5$ sintered body. The area of each number in (a) corresponds to the areas of same numbers in (b) and (c).

Figure S4. demonstrates the calculated electron diffraction patterns along <100> zone axis direction of cubic phase (i) and orthorhombic phase (ii) of $Ba_2In_2O_5$ brownmillerite.

(i) Cubic phase / *Pm3m* (221)   (ii) Orthorhombic phase / *Ima2* (46)
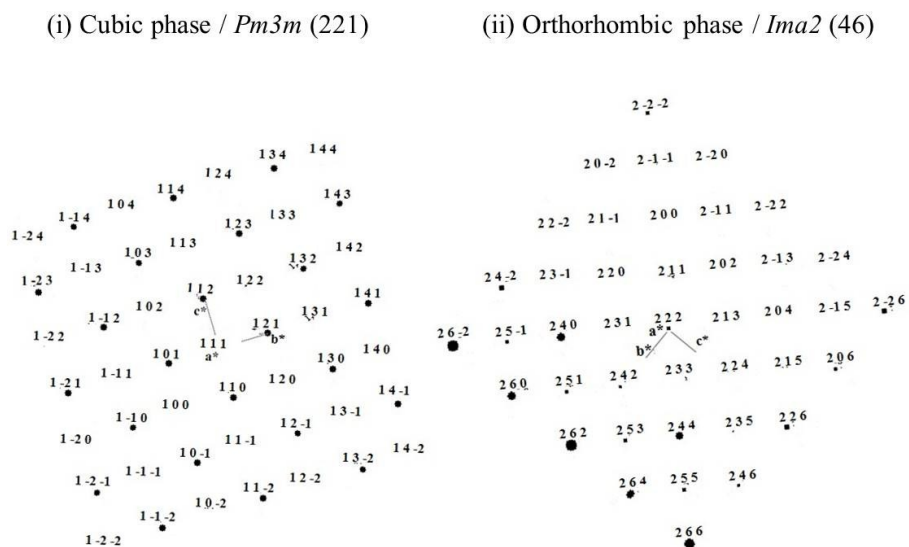
Figure S4. Calculated electron diffraction patterns along <100> zone axis direction of cubic phase (i) and orthorhombic phase (ii) of $Ba_2In_2O_5$ brownmillerite.

Figures S5a to S5e demonstrate the representative examples of unstable cluster models.

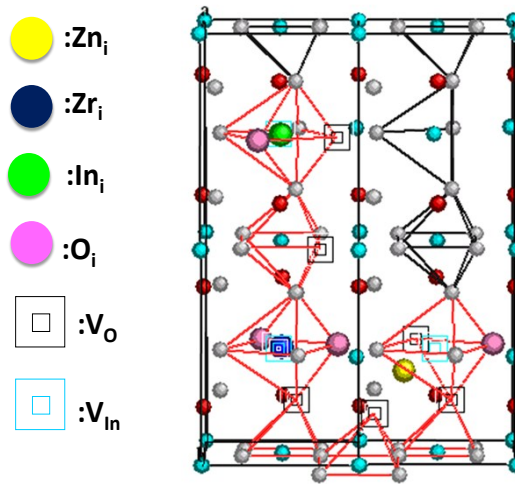Figure S5a. Unstable cluster model which consists of the improper defect positions.

Defect composition: $3V_{In}''' - In_i^{\cdots} - Zn_i^{\cdot\cdot} - Zr_i^{\cdots\cdot} - 4V_o^{\cdot\cdot} - 4O_i''$

Number of defects: 14, binding energy (ΔE_b): 0.8 eV

The position of interstitial site of Zn is too much close to Ba site as compared to stable cluster with proper positions of defects.
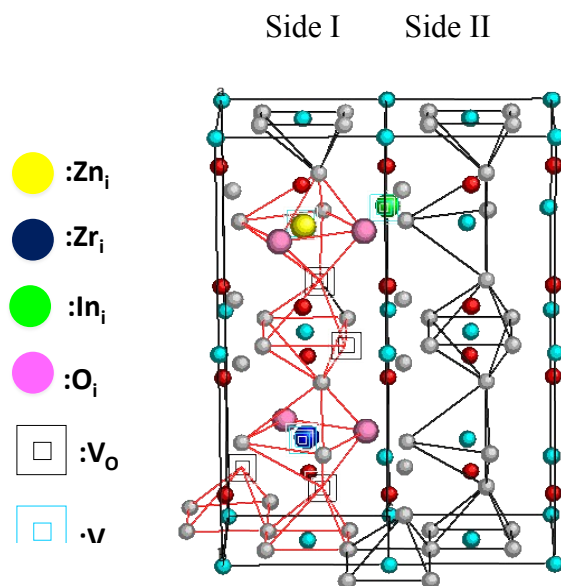
Figure S5b. Unstable cluster model which consists of the improper defect positions.

Defect composition: $3V_{In}''' - In_i^{\bullet\bullet\bullet} - Zn_i^{\bullet\bullet} - Zr_i^{\bullet\bullet\bullet\bullet} - 4V_o^{\bullet\bullet} - 4O_i''$

Number of defects: 14, binding energy (ΔE_b): 0.7 eV

In the case of proper defect positions in the stable cluster model, the position of Zr interstitial site locates in side I and Zn interstitial site position is in side II of unit cell. In contrast, both positions of Zr interstitial site and Zn interstitial site located in side I of unit cell when cluster model is unstable as shown in Figure S5b.
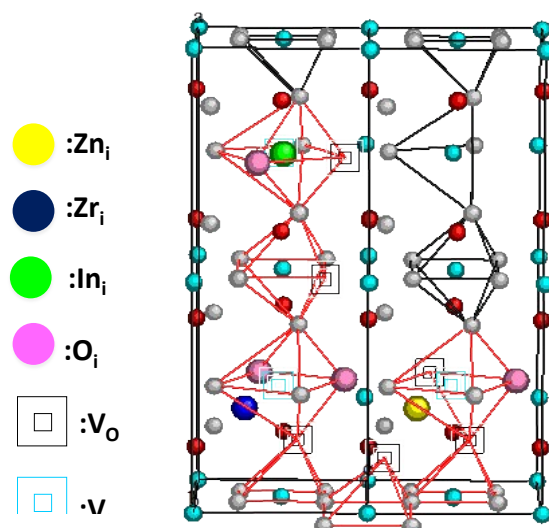
Figure S5c. Unstable cluster model which consists of the improper defect positions.

Defect composition: $3V_{In}''' - In_i^{\bullet\bullet\bullet} - Zn_i^{\bullet\bullet} - Zr_i^{\bullet\bullet\bullet\bullet} - 4V_o^{\bullet\bullet} - 4O_i''$

Number of defects: 14, binding energy (ΔE_b): 0.4 eV

Both positions of interstitial site of Zn and interstitial site of Zr are too much close to Ba site as compared to the stable cluster with proper positions of defects.
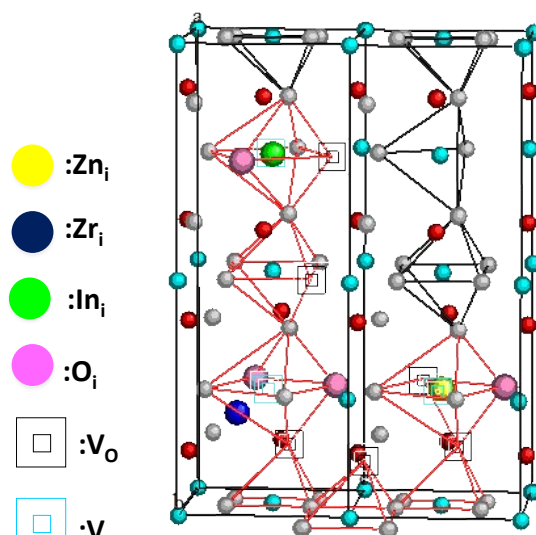
Figure S5d. Unstable cluster model which consists of the improper defect positions.

Defect composition: $3V_{In}''' - In_i^{\bullet\bullet\bullet} - Zn_i^{\bullet\bullet} - Zr_i^{\bullet\bullet\bullet\bullet} - 4V_o^{\bullet\bullet} - 4O_i''$

Number of defects: 14, binding energy (ΔE_b): 0.1 eV

The position of interstitial site of Zr is too much close to Ba site as compared to stable cluster with proper positions of defects.
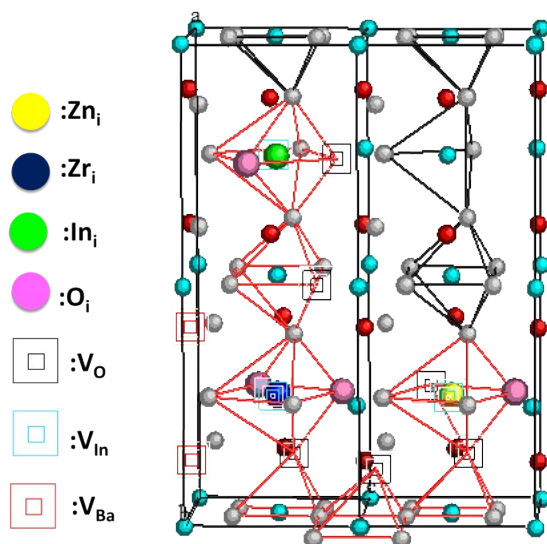
Figure S5e. Unstable cluster model which consists of the improper defect positions.

Defect composition: $3V_{In}''' - In_i^{\bullet\bullet\bullet} - Zn_i^{\bullet\bullet} - Zr_i^{\bullet\bullet\bullet\bullet} - 4V_o^{\bullet\bullet} - 4O_i'' - 2V_{Ba}''$

Number of defects: 16, binding energy (ΔE_b): - 2.7 eV

The excess Ba defects are involved in the unstable cluster model as shown in Figure S5e.

As shown in Figure S6(a), the number of hooping site (i.e. oxygen vacancy) which was formed in BIZZO-0.3 was two time higher than conventional BIO without dopants. Therefore, we conclude that the electrical conductivity observed for BIZZO-0.3 was two times higher than disordered state of BIO without dopants.

Also, the stable defect clusters ($3V_{In}''' - In_i^{\cdots} - Zn_i^{\cdot\cdot} - Zr_i^{\cdots\cdot} - 4O_i'' - 4V_o^{\cdot\cdot}$) which is the building unit of larger defect clusters in BIZZO-0.3 will create wide disordering area in microscopic scale for fast oxide ionic conduction as well as disordered state of BIO, as shown in Figure 6S(b).

(a)
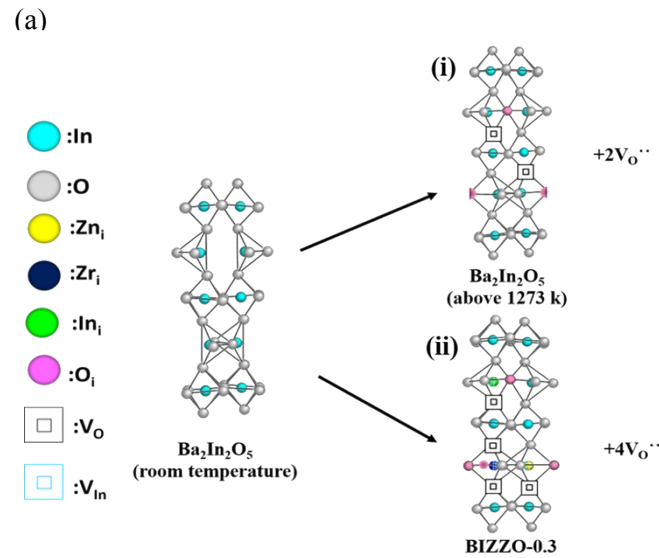
In the case of substitution of dopants such as di-valent Zn cation (i.e. Zn^{2+}) and tetra-valent Zr cation (i.e. Zr^{4+}) for In (III)-site, Zn^{2+} would substitute on the site of octahedral coordination (i.e. 6-fold coordination) of In (III) by oxygen in $Ba_2In_2O_5$ lattice. And Zr^{2+} would occupy the site of tetrahedral coordination (i.e. 4-fold coordination) of In (III) by oxygen in $Ba_2In_2O_5$ brownmillerite lattice.

If we assume aforementioned coordination of Zn^{2+} and Zr^{4+} in the lattice of $Ba_2In_2O_5$ brownmillerite (i.e. formation of Schottky type point defect structure), the defect structure of $Ba_2In_2O_5$ will be perovskite structure which is high temperature form of $Ba_2In_2O_5$ brownmillerite (see Figure S6 (a-i)). In that case, we cannot expect both of the preferable defect structure which is shown in Figure S6 (a-ii) (i.e. Frenkel type point

defect structure) and the enhancement of the ionic conductivity which is induced by formation of Frenkel type point defect structure. Therefore, it is conclude that the improved ionic conductivity was not observed by formation of Schottky type point defect structure in the previously reported $Ba_2In_2O_5$ doped with various kinds of dopant samples as compared with high temperature form of $Ba_2In_2O_5$. That is why the present work did not consider the formation of Schottky type point defect structure (i.e. substitution of dopants for In (III)-site) of $Ba_2In_2O_5$ brownmillerite lattice in our work.
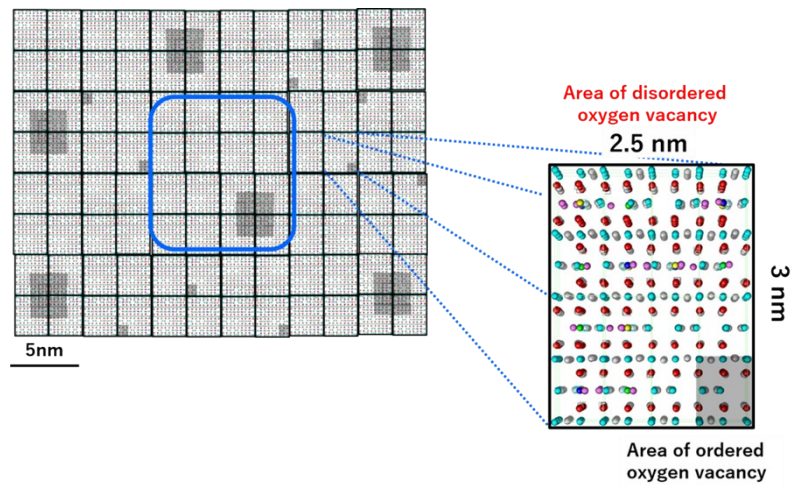
(b)

Figure S6. (a) Comparison of oxygen vacancy sites which were created in unite cell of disordered state of BIO and BIZZO-0.3, (b) schematic diagram for explanation of TEM image which was shown in Figure 7 and atomistic simulation shown in Figure 9.